fibers

MDPI

Article

Waste-Derived Oil Palm Mesocarp Fiber in LLDPE Biocomposites: Low-Loading Mechanical and Moisture Response

Muhammad Irfan Nuryanta [1,2,*], Rahmat Doni Widodo [1], Ahmad Mujaki [1], Hendrix Noviyanto Firmansyah [1,2], Rizky Ajie Aprilianto [3], Betti Ses Eka Polonia [2,4], Edi Purnomo [2], Urip Agus Salim [2], Gesang Nugroho [2] and Muhammad Akhsin Muflikhun [2]

[1] Department of Mechanical Engineering, Faculty of Engineering, Universitas Negeri Semarang, Semarang 50229, Indonesia
[2] Department of Mechanical and Industrial Engineering, Faculty of Engineering, Universitas Gadjah Mada, Jl. Grafika No. 2, Yogyakarta 55281, Indonesia
[3] Department of Electrical Engineering, Faculty of Engineering, Universitas Negeri Semarang, Semarang 50229, Indonesia
[4] Department of Mechanical Engineering, Politeknik Negeri Ketapang, Ketapang 78813, Indonesia
* Correspondence: irfannuryanta@mail.unnes.ac.id or irfannuryanta@mail.ugm.ac.id

Abstract

Waste-derived oil palm mesocarp fiber (OPMF) has potential as a lignocellulosic reinforcement for thermoplastic composites. The same trend in strength, stiffness, and moisture-related properties does not always hold at relatively low fiber loadings. This study examined these property changes in linear low-density polyethylene (LLDPE) biocomposites. Composites containing 0, 5, 10, and 15 wt% alkali-treated OPMF were produced by hot compression molding. Tensile and flexural properties, density, 24 h water absorption, and water contact angle were evaluated, supported by scanning electron microscopy (SEM), Fourier-transform infrared spectroscopy (FTIR), and differential scanning calorimetry (DSC). The 5 wt% composite showed the highest mean tensile and flexural strengths of 16.16 ± 1.14 MPa and 29.33 ± 3.57 MPa, while the highest apparent tensile modulus (521.25 ± 38.84 MPa) and flexural modulus (0.888 ± 0.122 GPa) occurred at 10 wt%. Water absorption increased from 0.06 ± 0.01% to 1.19 ± 0.12%, while the contact angle decreased from 97.78 ± 2.04° to 65.18 ± 5.21°. Strength, stiffness, and moisture response followed different loading-dependent trends, indicating a composition-dependent strength–stiffness–moisture trade-off within the investigated range.

Keywords: oil palm mesocarp fiber; linear low-density polyethylene; water absorption; contact angle; mechanical properties; moisture sensitivity

Check for updates

Academic Editor: Martin J. D. Clift

Received: 1 October 2026
Revised: 29 October 2026
Accepted: 5 November 2026
Published: 13 November 2026

Copyright: © 2026 by the authors. Licensee MDPI, Basel, Switzerland. This article is an open access article distributed under the terms and conditions of the Creative Commons Attribution (CC BY) license.

1. Introduction

The increasing demand for lightweight, more sustainable engineering materials has spurred the development of thermoplastic composites reinforced with renewable lignocellulosic materials [1–3]. Among these resources, considerable amounts of fibrous residues are generated during oil palm processing and remain attractive for conversion into value-added composite reinforcement [4]. The oil palm mesocarp fiber (OPMF) is especially attractive as it is renewable, lightweight and derived from a large agricultural residue [5], which makes its inclusion in polymer composites relevant from both material performance and resource-efficiency perspectives [6–9].

Linear low-density polyethylene (LLDPE) is widely used because of its flexibility, chemical resistance, and ease of processing [10]. However, it is relatively low in stiffness, which

limits its use in applications requiring greater rigidity [11]. The addition of lignocellulosic fibers into LLDPE is a practical approach to modify its mechanical behavior and partially substitute the petroleum-based polymer with a renewable reinforcement. But the mix is not easy. The hydrophilicity of the lignocellulosic fibers contrasts with the hydrophobic nature of polyethylene, which may result in interfacial debonding, fiber pull-out, and non-uniform stress transfer. Therefore, alkali treatment is widely used to modify the fiber surface before incorporating it into polyolefin matrices [12].

Alkali treatment is commonly used as a fiber-preparation step to remove surface impurities and modify the lignocellulosic surface before compounding [13,14]. In the present work, all OPMF-containing formulations received the same 5% (w/v) NaOH treatment; therefore, the experiment was designed to evaluate fiber-loading effects rather than to quantify the independent effect of alkali treatment. Fracture morphology and moisture uptake were evaluated as complementary indicators of the resulting material response.

The effect of fiber loading can differ between tensile and flexural deformation and need not follow the same trend as moisture uptake [15–17]. Tensile response is sensitive to stress-transfer continuity and localized fracture initiation, whereas flexural loading develops tensile and compressive stress gradients across the specimen thickness. At the same time, increasing lignocellulosic content generally introduces more hydrophilic domains that can affect short-term water absorption [18]. Consequently, a formulation that provides the most favorable tensile response may not maximize flexural performance or minimize moisture sensitivity.

Accordingly, this study investigates the fiber-loading-dependent mechanical and moisture performance of LLDPE biocomposites containing 0, 5, 10, and 15 wt% alkali-treated oil palm mesocarp fiber. The primary objective is to determine how OPMF loading is associated with tensile and flexural response and 24 h water absorption under fixed fiber-treatment and processing conditions. Experimental density, selected SEM fracture morphology, FTIR features, DSC transitions, and statistical analysis are used as supporting characterization to contextualize the measured performance trends without attributing them to mechanisms that were not independently measured.

Table 1 shows the position of the present study compared with previous work on OPMF-based composites. Earlier studies have generally discussed mechanical performance, interfacial characteristics, fiber treatment, or water absorption, often using other polymer matrices or relatively high fiber contents. The present study focused on a relatively low OPMF content in LLDPE, with the treatment and processing parameters kept unchanged for all formulations. The resulting composites were evaluated for mechanical performance, water uptake, surface wettability, thermal characteristics, and fracture morphology. The comparison indicates that the contribution of this work is not limited to using OPMF as a reinforcement in LLDPE, but also to demonstrating that strength, stiffness, and moisture-related behavior do not change in the same way as fiber content increases. This provides a clearer picture of the balance between mechanical improvement and increasing moisture sensitivity within the investigated loading range.

Table 1. Research Gap and Novelty Positioning of Waste-Derived OPMF/LLDPE Biocomposites.

Study	Matrix	Main Variable	Key Finding	Research Gap/Novelty Position
Olusunmade et al. [19]	LLDPE	OPMF, 5–25 wt%	Modulus increased, while tensile strength decreased with increasing loading.	Focused on mechanical properties and SEM, without assessing flexural, moisture, wettability, or thermal responses.

Table 1. *Cont.*

Study	Matrix	Main Variable	Key Finding	Research Gap/Novelty Position
Hanipah et al. [20]	LLDPE	OPMF interface/silica bodies	Silica bodies influenced fiber pull-out and interfacial behavior.	Focused on interface mechanisms rather than low-loading multi-property trade-offs.
Huisken et al. [8]	Polyester	OPMF loading	Fiber loading changed mechanical response and increased water uptake.	Thermoset matrix; surface wettability and LLDPE crystallinity were not examined.
Saepoo et al. [6]	Thermoplastic starch	Waste OPMF loading	Waste OPMF altered mechanical and water-related behavior and enabled residue valorization.	Different hydrophilic matrix and much higher fiber loading than the present LLDPE system.
Present work	LLDPE	0, 5, 10, 15 wt% waste-derived OPMF	5 wt% gave the highest mean strength; 10 wt% gave the highest stiffness; higher loading increased wettability and water uptake.	Integrates mechanical, moisture, wettability, thermal, and morphological analyses, revealing distinct strength–stiffness–moisture trends.

2. Materials and Methods

2.1. Materials, Fiber Treatment, and Composite Fabrication

Linear Low-Density Polyethylene (LLDPE), TITANVENE® from LOTTE Chemical Titan (Pasir Gudang, Malaysia), was used as the thermoplastic matrix. Oil palm mesocarp fiber (OPMF), collected as a fibrous waste residue from oil palm processing, was used as the lignocellulosic reinforcement. The fiber length used for composite preparation was approximately 3 mm.

Before composite fabrication, the OPMF was treated in a 5% (w/v) sodium hydroxide (NaOH) aqueous solution prepared with distilled water. A fiber-to-solution ratio of 1:25 (w/v) was maintained, and the fibers were immersed for 2 h. After alkali treatment, the fibers were thoroughly rinsed with distilled water to remove residual NaOH. The washed fibers were left to drain at room temperature for 24 h, followed by oven drying at 60 °C for 2 h. They were then stored in sealed containers until composite fabrication. The same treatment and drying procedures were applied to all OPMF-containing formulations. The preparation of OPMF and the fabrication process of LLDPE/OPMF biocomposites are illustrated in Figure 1.

Four formulations containing 0, 5, 10, and 15 wt% OPMF were prepared, with fiber content calculated relative to the total composite mass (Table 2). The required LLDPE and treated OPMF were premixed using a mechanical stirrer at 100 rpm for 2 min, with the fiber introduced before the LLDPE was fully softened [21]. The premix was heated in an oven at 160 °C for a total of 30 min. After the first 15 min, the partially softened blend was removed and manually kneaded with a spatula for 2 min to redistribute the fiber, then returned to the oven for an additional 15 min. Immediately after preheating, the softened material was transferred to a preheated steel mold and consolidated by hot compression molding at 160 °C under a pressing force of 2 ton-force for approximately 10 min. The composite was cooled while remaining inside the mold before demolding. Plates with nominal in-plane dimensions of 150 × 150 mm and a nominal thickness of approximately 4 mm were produced. The actual specimen thickness was measured individually, and the measured value was used in mechanical calculations.

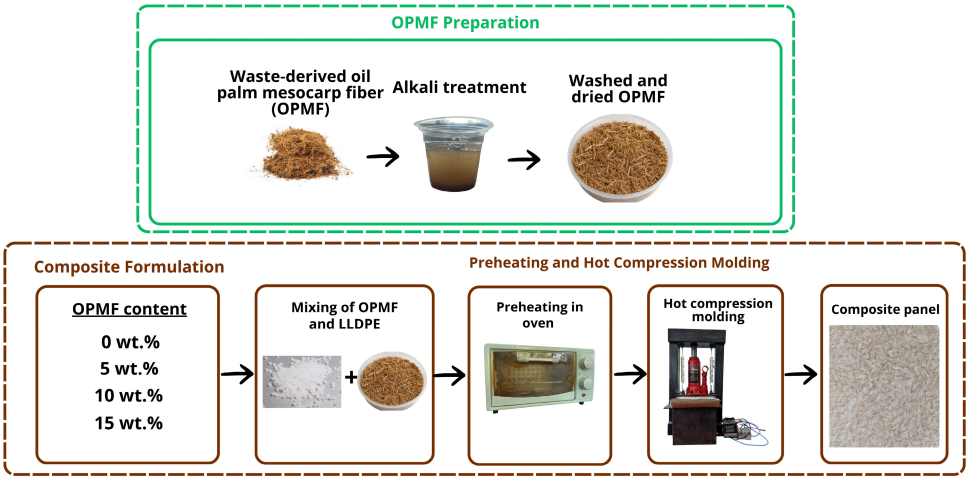


Figure 1. Schematic illustration of waste-derived oil palm mesocarp fiber (OPMF) preparation and fabrication of LLDPE/OPMF biocomposites by hot compression molding.

Table 2. Formulations of LLDPE/OPMF composites.

Sample	LLDPE (wt%)	OPMF (wt%)
LLDPE	100	0
LLDPE/OPMF 5%	95	5
LLDPE/OPMF 10%	90	10
LLDPE/OPMF 15%	85	15

2.2. Density and Water Absorption

Experimental density was determined from the dry specimen mass and measured specimen volume. Three measurements were used for each formulation, and the results are reported as means ± standard deviation [22]. Water absorption was evaluated after 24 h immersion in distilled water at room temperature. Dried specimens were weighed before immersion, removed after 24 h, gently wiped to remove surface water, and reweighed. Water absorption was reported as the percentage mass increase relative to the initial dry mass. Three specimens were evaluated for each formulation, and the values are reported as means ± standard deviation. The 24 h measurement is interpreted as short-term moisture uptake rather than long-term durability [23].

2.3. Water Contact Angle Measurement

Surface wettability was evaluated by measuring the apparent water contact angle using a contact angle goniometer (Ossila L2004A1, Sheffield, UK) [24]. A 10 µL water droplet was deposited onto the molded surface of each specimen, and its profile was recorded with the goniometer. The contact angle was determined at approximately 15 s after droplet deposition, when the droplet profile had become relatively stable. Measurements were performed on neat LLDPE and LLDPE/OPMF composites containing 5, 10, and 15 wt% OPMF. Five measurements were taken at different positions on the surface of each formulation to account for local surface variation. The droplet profiles were analyzed using Ossila Contact Angle software (version 4.2.2; Ossila Ltd., Sheffield, UK), and the results are reported as means ± standard deviation.

2.4. Tensile Testing

Tensile testing was performed using Type IV dog-bone specimens based on ASTM D638 [25] on a Carson universal testing machine (Jinan, China) with a 50 kN capacity.

Specimens were tested for each formulation at a constant crosshead speed of 2 mm/min after conditioning at room temperature [26]. Tensile strength was defined as the maximum engineering stress. Engineering strain was derived from crosshead displacement; therefore, the initial slope is reported as an apparent tensile modulus. Strain at maximum tensile stress was determined at the point of maximum engineering stress.

2.5. Flexural Testing

Three-point flexural tests were carried out using the same Carson 50 kN universal testing machine, using a three-point configuration based on ASTM D790 [27], with three specimens per formulation. The support-span-to-thickness ratio was maintained at 16:1 using the individually measured specimen thickness; the corresponding nominal span for the tested plates was approximately 64 mm. The crosshead rate was selected in accordance with ASTM D790 for the specimen geometry. Nominal flexural stress and outer-surface strain were determined from the recorded load–displacement response and actual specimen dimensions. Flexural modulus was obtained from the initial linear region of the flexural response [28].

2.6. SEM, FTIR, and DSC Characterization

Scanning electron microscopy was performed using a Thermo Scientific Phenom ProX (Eindhoven, The Netherlands) to examine the fracture morphology of the LLDPE/OPMF composites. Fragments were collected from the fracture regions of the mechanically tested specimens. The samples were mounted on aluminum stubs using conductive carbon tape and sputter-coated with a thin gold layer to minimize charging during imaging. The SEM micrographs were used for qualitative assessment of features such as exposed fibers, fiber pull-out, interfacial separation, matrix tearing, and cavity-like regions [29].

FTIR analysis was performed using a Shimadzu IRXross FTIR spectrophotometer (Shimadzu Corporation, Kyoto, Japan) to examine the chemical characteristics of neat LLDPE and LLDPE/OPMF composites. Spectra were acquired in the mid-infrared region using an FTIR spectrometer under the instrument's default acquisition settings. The FTIR data were recorded as percent transmittance (%T) as a function of wavenumber (cm^{-1}). Spectra of neat LLDPE and composites containing 5, 10, and 15 wt% OPMF were compared to identify changes in the characteristic absorption bands associated with the incorporation of lignocellulosic OPMF into the LLDPE matrix. For presentation, the spectra were vertically offset to improve visual clarity without altering the spectral features [30].

Differential scanning calorimetry was performed using a Shimadzu DSC-60A (Shimadzu Corporation, Japan) to evaluate the melting and crystallization behavior of neat LLDPE and LLDPE/OPMF composites containing 5, 10, and 15 wt% OPMF. Approximately 8–9 mg of each sample was placed in an alumina pan and analyzed under a nitrogen atmosphere at a flow rate of 30 mL/min. The samples were heated from 25 to 210 °C at 10 °C/min, held at 210 °C for 3 min, and then cooled to 25 °C at the same rate. The melting temperature (Tm) and crystallization temperature (Tc) were determined from the peak positions of the DSC heating and cooling curves, respectively. These parameters were used to evaluate changes in the principal thermal transition temperatures of LLDPE following OPMF incorporation [31].

2.7. Statistical Analysis

Results are reported as means ± standard deviations. One-way analysis of variance (ANOVA) was used to evaluate the effect of OPMF loading on the mechanical properties at a significance level of 0.05. For tensile and flexural strength, specimen-level data were additionally evaluated using Tukey's honestly significant difference (HSD) test after a

significant ANOVA result. Density and 24 h water absorption are reported descriptively as means ± standard deviations because the retained analysis did not use specimen-level inferential statistics for these physical properties. Statistical conclusions are interpreted together with the limited replicate number of three specimens per formulation.

3. Results and Discussion

3.1. Experimental Density, Water Absorption, and Surface Wettability

Experimental density and 24 h water absorption were evaluated as complementary physical responses to increasing OPMF content (Figure 2). Density increased gradually from 0.931 ± 0.005 g cm^{-3} for neat LLDPE to 0.973 ± 0.012 g cm^{-3} for LLDPE/OPMF-15. The increase was modest but systematic across the tested formulations and is consistent with the changing mass fraction of the lignocellulosic phase and the molded composite structure [18]. Huisken Mejouyo et al. [32] reported an OPMF density of 1.268 ± 0.112 g/cm^3, which is higher than that of neat LLDPE in this study (0.931 ± 0.005 g/cm^3). This difference may partly explain the increase in composite density with OPMF loading, although fiber distribution and possible voids may also affect the results. Formulation-dependent density changes have also been reported for polyethylene composites containing palm-derived or other natural reinforcements.

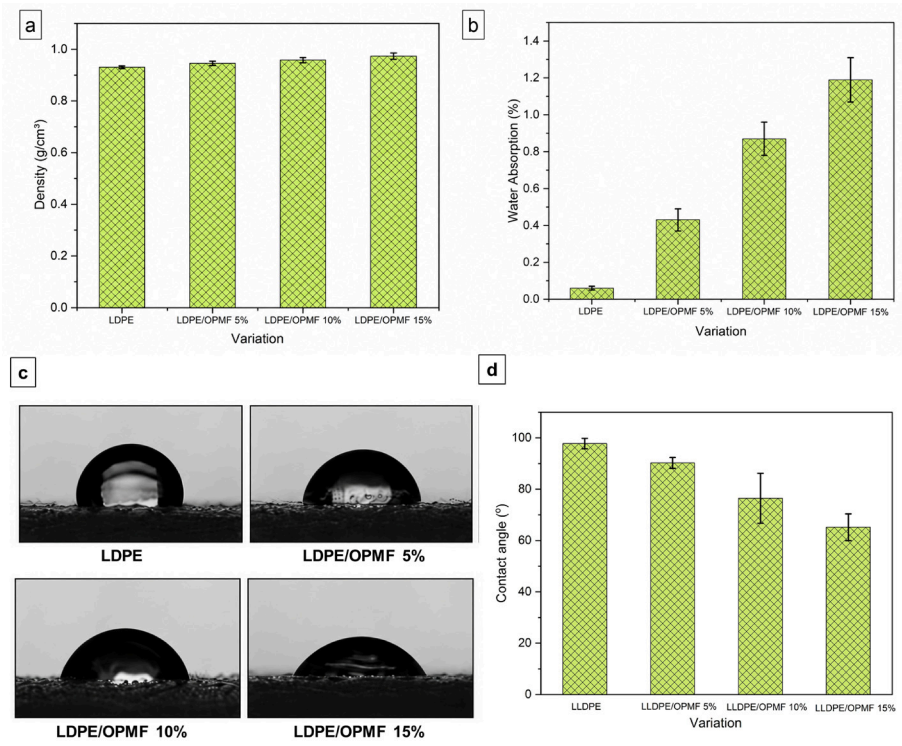


Figure 2. Physical properties of neat LLDPE and LLDPE/OPMF biocomposites at different fiber loadings: (**a**) experimental density; (**b**) 24 h water absorption; (**c**) representative water droplet images used for contact angle measurements, and (**d**) apparent water contact angle.

The moisture response showed a clearer monotonic trend than the mechanical properties. Water absorption increased from 0.06 ± 0.01% in neat LLDPE to 0.43 ± 0.06%, 0.87 ± 0.09%, and 1.19 ± 0.12% at 5, 10, and 15 wt% OPMF, respectively. This trend is compatible with the increasing fraction of hydroxyl-containing lignocellulosic domains and possible interfacial pathways for moisture access [28]. Because only a 24 h immersion period was evaluated, the results describe short-term moisture susceptibility and should not be extrapolated to long-term water transport or environmental durability.

The water contact angle decreased as the OPMF content increased. Neat LLDPE showed the highest value, 97.78 ± 2.04°, while the values for the 5, 10, and 15 wt% composites were 90.24 ± 2.13°, 76.46 ± 9.73°, and 65.18 ± 5.21°, respectively. This shows that the surface became easier to wet after OPMF was added. The trend is reasonable because OPMF contains more polar lignocellulosic groups, whereas LLDPE is primarily nonpolar. This is also consistent with the FTIR results, in which O–H and C–O-related bands became more prominent in the OPMF-containing samples. Still, the contact angle can also be affected by the local surface condition, such as roughness and the amount of fiber exposed at the surface.

A similar tendency was seen between the contact angle and water absorption results. As the contact angle became lower, the 24 h water uptake increased from 0.06% for neat LLDPE to 0.43%, 0.87%, and 1.19% for the composites containing 5, 10, and 15 wt% OPMF. This suggests that the surface became more susceptible to wetting as the fiber content increased, which was followed by greater water uptake. The larger scatter observed for the 10 wt% sample may be linked to differences in the local surface condition, such as uneven fiber exposure or surface texture. Although contact angle primarily describes wetting behavior at the surface, it should not be used as a direct indicator of moisture absorbed throughout the composite.

3.2. Tensile Response

Figure 3 shows that OPMF incorporation improved the tensile response of LLDPE, although the effect was not proportional to fiber loading. The highest mean tensile strength was obtained at 5 wt% OPMF (16.16 ± 1.14 MPa), approximately 54.7% higher than neat LLDPE (10.44 ± 1.43 MPa). Further increasing OPMF to 10 and 15 wt% slightly reduced the mean tensile strength, although both formulations remained stronger than neat LLDPE. This indicates that a relatively low fiber loading provided a favorable balance between reinforcement and continuity of the polymer matrix [33].

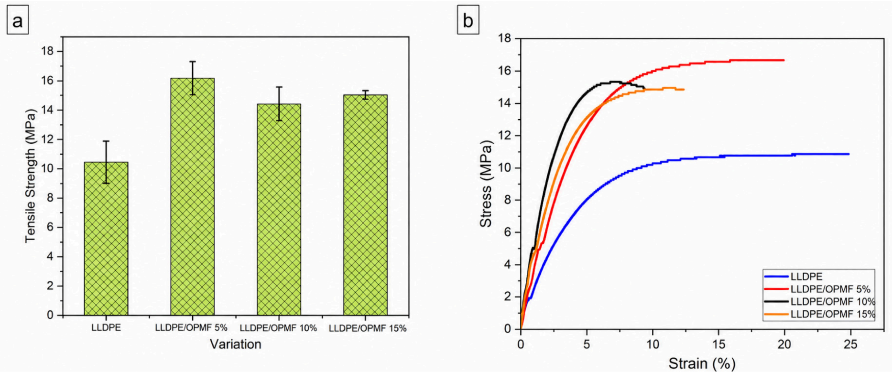


Figure 3. Tensile response of neat LLDPE and LLDPE/OPMF biocomposites: (**a**) mean tensile strength and (**b**) representative engineering stress–strain curves at different OPMF loadings.

The representative stress–strain curves further show that neat LLDPE exhibited the lowest stress level but the greatest deformation range, characteristic of a more ductile matrix [34,35]. The 5 wt% OPMF composite combined higher stress with relatively large deformation, whereas the 10 wt% formulation displayed a steeper initial response and lower strain, indicating increased apparent stiffness but reduced deformation capacity. At 15 wt% OPMF, the tensile response remained higher than neat LLDPE but did not exceed that of the 5 wt% formulation.

The reduction in performance beyond 5 wt% can be associated with increasing fiber–matrix interfaces and greater structural heterogeneity. At higher fiber contents, reduced

matrix continuity, local fiber-rich regions, interfacial separation, and fiber pull-out may generate stress concentrations and limit efficient load transfer [3,36,37]. These interpretations are qualitatively consistent with the SEM observations, but the morphology should be treated as supporting evidence rather than direct proof of the governing failure mechanism.

Statistically, formulation significantly affected tensile strength ($p = 0.001$). However, although 5 wt% OPMF showed the highest mean value, the differences among the 5, 10, and 15 wt% OPMF formulations were not statistically significant. Therefore, 5 wt% should be described as the formulation with the highest mean tensile strength, rather than as a statistically confirmed optimum.

The apparent tensile modulus increased from 191.51 ± 34.73 MPa for neat LLDPE to 307.44 ± 59.43 MPa at 5 wt% OPMF. The highest mean value was recorded at 10 wt% (521.25 ± 38.84 MPa), before decreasing to 396.37 ± 55.64 MPa at 15 wt%. This indicates that the stiffness response did not increase continuously with increasing fiber content. The distinction is mechanically reasonable because tensile modulus is the measure of initial resistance to deformation [38] and tensile strength is the measure of maximum stress sustained by the composite [1,39]. The higher OPMF content at 10 wt % resulted in a higher amount of relatively stiff lignocellulosic reinforcement, which restricted matrix deformation and increased the initial stiffness [40]. However, this formulation also had the lowest strain at maximum stress (6.79 ± 0.96%), indicating a more stiffness-dominated and deformation-limited response. The lack of a corresponding increase in tensile strength suggests that the stiffening effect at 10 wt % was accompanied by interfacial and microstructural heterogeneity that were composition-dependent and limited the maximum load-bearing capability.

3.3. Flexural Response

Figure 4a represents the flexural strength of neat LLDPE and LLDPE/OPMF biocomposites. The inclusion of OPMF resulted in a non-monotonic change in flexural performance. The mean value of flexural strength of neat LLDPE was 24.38 ± 4.60 MPa, and the addition of 5 wt% OPMF increased the mean value to 29.33 ± 3.57 MPa, which is an increase of about 20.3%. Increasing the fiber content to 10 wt. % further resulted in a slightly lower flexural strength of 27.90 ± 2.44 MPa. The 15 wt. % formulation yielded 25.28 ± 3.25 MPa, which was close to the response of neat LLDPE. The maximum average flexural strength was observed at 5 wt% OPMF, while the improvement was not directly proportional to fiber loading [41,42].

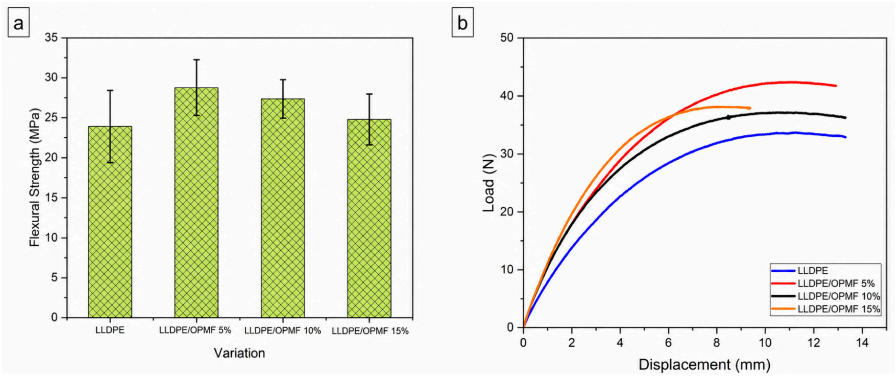


Figure 4. Flexural response of neat LLDPE and LLDPE/OPMF biocomposites: (**a**) mean flexural strength and (**b**) representative load–displacement curves at different OPMF loadings.

The increase in the mean flexural strength at 5 wt% OPMF indicates a positive balance between the reinforcing contribution of OPMF and the continuity of the LLDPE matrix at a relatively low fiber content. In three-point bending, tensile and compressive stresses occur

simultaneously throughout the specimen's thickness [43]. At moderate fiber content, the relatively stiff lignocellulosic fibers can restrict local matrix deformation and contribute to load transfer, while sufficient polymer remains available to surround the reinforcement [44–46]. Consequently, the average bending stress for the 5 wt% formulation was higher before reaching the maximum load.

Increasing the OPMF content beyond 5 wt% did not further increase flexural strength. At higher fiber fractions, the increasing number of fiber–matrix interfaces, reduced local matrix continuity, and greater microstructural heterogeneity can reduce the efficiency of stress transfer [47]. The SEM observations provide qualitative support for this interpretation, showing fiber pull-out, interfacial separation, and cavity-like regions, with more pronounced local interfacial discontinuities at higher OPMF contents. However, these morphological observations should be regarded as supporting evidence rather than direct proof of the governing failure mechanism.

The flexural modulus exhibited a somewhat different response from flexural strength. Neat LLDPE showed a modulus of 0.596 ± 0.190 GPa, which increased to 0.808 ± 0.138 GPa at 5 wt% OPMF and reached the highest mean value of 0.888 ± 0.122 GPa at 10 wt% OPMF. At 15 wt% OPMF, the modulus decreased to 0.700 ± 0.150 GPa but was still higher than that of the neat LLDPE. The mean flexural modulus increased by about 35.7%, 49.1% and 17.6% for the formulations of 5, 10 and 15 wt. % compared to the neat matrix.

The difference between the fiber loading corresponding to maximum strength and maximum stiffness is of mechanical significance. Flexural strength is the maximum stress before peak load, while flexural modulus is the resistance to deformation in the initial linear region. The higher modulus at 10 wt. % indicates that the addition of relatively rigid OPMF was more effective in restricting initial matrix deformation. However, the increase in flexural strength was not proportional. Thus, the increase in stiffness with this loading was tempered by factors limiting the maximum load-bearing capability [48].

Statistical analysis showed that OPMF loading did not produce a statistically significant difference in flexural strength (one-way ANOVA, $p = 0.354$) despite the approximately 20% increase in the mean value at 5 wt% OPMF. Similarly, the variation in flexural modulus was not statistically significant ($p = 0.177$). Therefore, the 5 wt% formulation should be described as having the highest mean flexural strength, and the 10 wt% formulation as having the highest mean flexural modulus, rather than as statistically confirmed optima. The results nevertheless indicate a clear composition-dependent trend in which moderate OPMF incorporation improved the average bending strength and stiffness, followed by diminished mechanical benefit at 15 wt% fiber loading.

3.4. Fracture Morphology

The SEM micrograph of neat LLDPE in Figure 5a shows a relatively continuous matrix with fibrillar structure, matrix tearing, and a cavity-like region, indicating ductile deformation of the polymer during tensile loading. In Figure 5b, a clear gap is visible around the fiber, while most of the surrounding LLDPE matrix still appears relatively continuous. Although local debonding was already present, the lower fiber content likely allowed the polymer matrix to remain sufficiently continuous to carry the applied load. This may explain why the 5 wt% composite retained the highest mean tensile and flexural strengths. A different fracture appearance can be seen in Figure 5c, where several fibers remain embedded in the matrix and are accompanied by noticeable matrix tearing. These features suggest stronger local mechanical interaction between the fibers and LLDPE, so that fracture did not occur only by simple fiber separation. This morphology agrees well with the increase in stiffness at 10 wt% OPMF, where the highest tensile and flexural moduli were obtained. The rougher and more deformed matrix around the fibers also suggests that part of the applied stress

was transferred through the fiber–matrix region before final fracture [49]. Nevertheless, the fracture surface is still heterogeneous, indicating that interfacial bonding was not uniform throughout the composite.

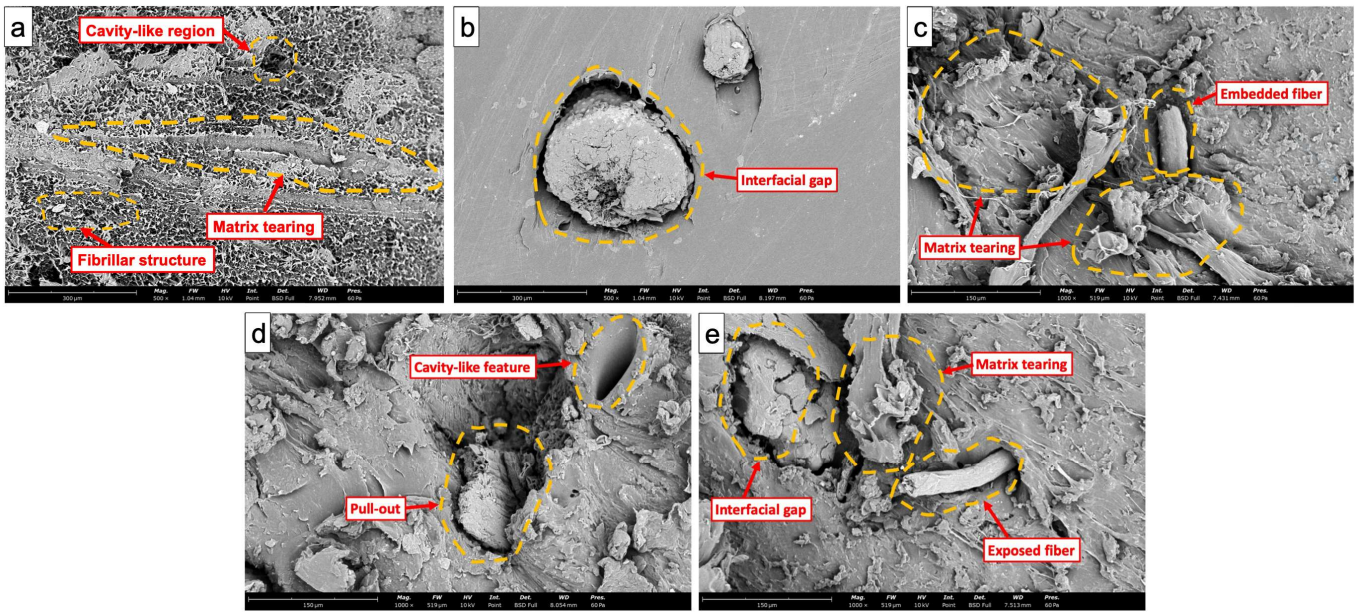


Figure 5. SEM micrographs of tensile fracture surfaces of (**a**) neat LLDPE and LLDPE/OPMF composites containing (**b**) 5 wt%, (**c**) 10 wt%, and (**d**,**e**) 15 wt% OPMF.

When the OPMF content increased further, interfacial defects became more evident. Figure 5d shows fiber pull-out together with a cavity-like region that was probably left after fiber detachment, whereas Figure 5e contains interfacial gaps, exposed fibers, and locally torn matrix. The increasing occurrence of these features indicates that some fibers were no longer effectively constrained by the LLDPE matrix during loading. At higher fiber contents, closer fiber spacing, incomplete wetting, and local fiber-rich regions may therefore have promoted debonding and pull-out instead of effective stress transfer. This provides a reasonable microstructural explanation for the reduction in tensile and flexural strength after the low-loading condition, as well as the decrease in flexural modulus at 15 wt% compared with 10 wt% OPMF. The SEM observations are also in line with the FTIR results, where no distinct evidence of new covalent bonding between OPMF and LLDPE was detected. Thus, the mechanical response appears to depend mainly on physical contact, mechanical interlocking, matrix continuity, and the local quality of the fiber–matrix interface. At the same time, the relatively small changes in melting and crystallization temperatures obtained from DSC indicate that the basic thermal-transition behavior of LLDPE was largely maintained after OPMF addition. Taken together, these results suggest that the variation in mechanical properties was governed more by fiber loading and the resulting interfacial and fracture morphology than by a major change in the chemical or thermal structure of the polymer matrix.

3.5. FTIR Analysis

Figure 6 presents the FTIR spectra of neat LLDPE and LLDPE/OPMF biocomposites at different fiber loadings, together with the spectra of untreated and alkali-treated OPMF. The characteristic absorption bands of the polyethylene matrix dominated the FTIR spectra of neat LLDPE and LLDPE/OPMF composites. The neat LLDPE showed strong bands at 2914–2916 and 2847–2849 cm^{-1}, which are attributed to asymmetric and symmetric CH_2 stretching, respectively, and bands at 1462–1464 and 717–719 cm^{-1}, which are due to CH_2

deformation and rocking vibrations, respectively. The characteristic bands of polyethylene were still observed in the composites containing OPMF, suggesting that the basic chemical structure of LLDPE was preserved after the introduction of the fiber.

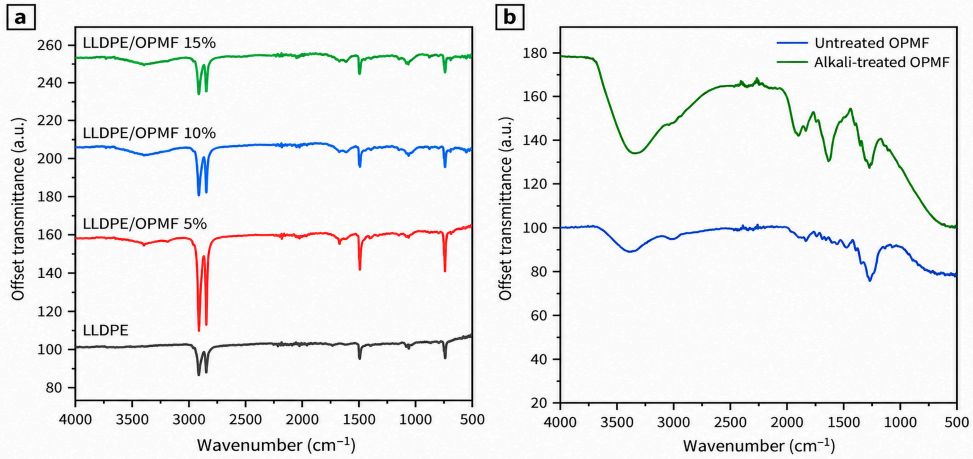


Figure 6. FTIR spectra of (**a**) neat LLDPE and LLDPE/OPMF biocomposites containing 5, 10, and 15 wt% OPMF, and (**b**) untreated and alkali-treated OPMFs.

Compared with neat LLDPE, the spectra of the 5, 10 and 15 wt% OPMF composites showed weak lignocellulosic-related features, including a broad absorption around 3393–3395 cm^{-1} associated with O–H stretching and features within approximately 1020–1160 cm^{-1} attributable to C–O and C–O–C vibrations of polysaccharide-containing constituents. These features are consistent with the presence of lignocellulosic OPMF within the LLDPE matrix and are also compatible with the observed increase in water absorption as the fiber content increased [50,51].

Importantly, no distinct new absorption bands or substantial shifts in the principal LLDPE bands were observed after OPMF incorporation. Therefore, the FTIR results do not provide evidence of new covalent bond formation between LLDPE and OPMF under the processing conditions used. Instead, the spectra indicate the coexistence of polyethylene and lignocellulosic functional groups within the composites. The comparison between untreated and alkali-treated OPMF in Figure 6b revealed changes in the O–H, C–H, and C–O-related absorption regions, suggesting modifications in the chemical environment of the lignocellulosic constituents following NaOH treatment. Previous studies have reported that NaOH treatment can remove surface impurities and part of the non-cellulosic components, which may change the fiber surface and its interaction with the polymer matrix [52]. However, these spectral changes do not provide quantitative evidence of hemicellulose or lignin removal, nor do they directly establish improved fiber–matrix interfacial bonding.

3.6. DSC Thermal Response

The DSC results presented in Figure 7 and Table 3 indicate that the incorporation of OPMF had a relatively limited influence on the melting and crystallization temperatures of LLDPE. Neat LLDPE exhibited a melting temperature (Tm) of 126.94 °C, while the biocomposites containing 5, 10, and 15 OPMF showed values of 127.31, 126.71, and 126.03 °C, respectively. The small variations in Tm suggest that the addition of OPMF did not substantially alter the principal melting transition of the LLDPE matrix [53].

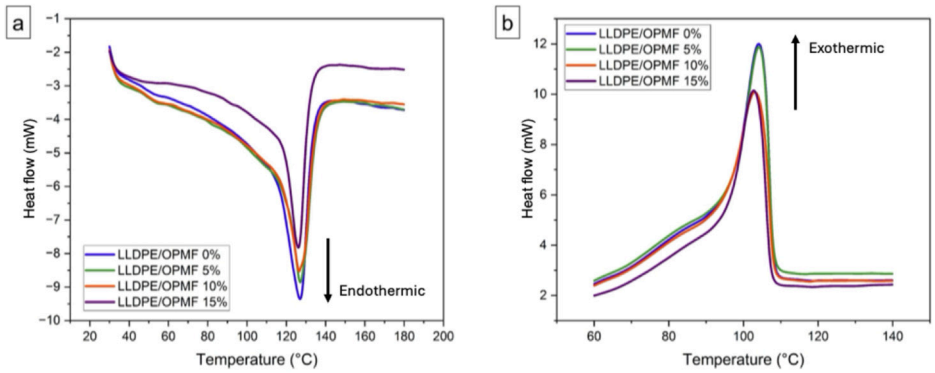


Figure 7. DSC (**a**) heating and (**b**) cooling curves of neat LLDPE and LLDPE/OPMF composites containing 5, 10, and 15 wt% OPMF.

Table 3. DSC-derived thermal parameters of neat LLDPE and LLDPE/OPMF composites.

OPMF Content (wt%)	Tm (°C)	Tc (°C)
0	126.94	104.17
5	127.31	104.16
10	126.71	103.02
15	126.03	102.89

The crystallization temperature (Tc) decreased slightly from 104.17 °C for neat LLDPE to 104.16, 103.02, and 102.89 °C for the composites containing 5, 10, and 15 wt% OPMF, respectively. This modest reduction may reflect changes in crystallization behavior associated with the presence of lignocellulosic fibers. However, the observed temperature shifts alone are insufficient to establish whether OPMF promotes or restricts the overall crystallization of LLDPE.

A broad shoulder-like feature was also observed around 80–90 °C in the cooling curves. This feature was not clearly resolved as a separate crystallization peak and may be associated with a broader distribution of crystallization processes or baseline-related effects. Therefore, it was not assigned to an independent thermal transition.

3.7. Integrated Structure–Property Relationships

The effect of OPMF addition on LLDPE biocomposites was not the same for all the properties examined. At 5 wt% OPMF, the highest mean tensile and flexural strengths were recorded, with values of 16.16 ± 1.14 MPa and 29.33 ± 3.57 MPa, respectively. Meanwhile, the highest apparent tensile modulus (521.25 ± 38.84 MPa) and flexural modulus (0.888 ± 0.122 GPa) were found at 10 wt%. This shows that the fiber content associated with higher strength was not necessarily the same as that giving higher stiffness [54]. However, these results represent differences in the measured mean values and should not be taken as evidence of a statistically confirmed optimum composition.

Some differences were also seen in the SEM images. At lower OPMF contents, the LLDPE matrix still appeared fairly continuous, although small gaps were visible around several fibers. When the fiber content reached 10 wt%, matrix tearing became more noticeable, with some fibers remaining embedded in the polymer. This may be related to local stress transfer between the fibers and matrix [55]. At higher OPMF loading, the fracture surfaces showed more exposed fibers, pull-out, and cavities, along with gaps at the fiber–matrix interface. Such features may contribute to less effective stress transfer and could partly explain the lower strength at higher fiber contents [56]. Still, these are observations from

local fracture areas, so the SEM images alone cannot confirm how strong the interfacial bonding actually was.

A more consistent trend was observed for the moisture-related properties. Water absorption increased from 0.06 ± 0.01% in neat LLDPE to 1.19 ± 0.12% at 15 wt% OPMF. Over the same range, the apparent contact angle decreased from 97.78 ± 2.04° to 65.18 ± 5.21°. The increase in water absorption is likely related to the hydrophilic character of OPMF, which contains polar functional groups also identified in the FTIR analysis. In addition, gaps around the fibers and exposed fiber surfaces may provide possible pathways for water to enter the composite. However, the available results do not show how much each of these factors contributed to moisture uptake.

From the DSC results, only slight differences were found in the melting and crystallization temperatures. The melting temperatures ranged from 126.03 to 127.31 °C, while the crystallization temperatures were between 102.89 and 104.17 °C. These small changes suggest that the main thermal transition temperatures of LLDPE were largely retained after OPMF addition. Crystallinity may also play a role in the mechanical response, but changes in crystallinity cannot be determined from these peak temperatures alone. For this reason, the higher apparent stiffness at 10 wt% OPMF cannot be directly linked to an increase in crystallinity.

Taken together, the results suggest that adding OPMF involves a balance between mechanical performance and moisture resistance. Moderate fiber content yielded higher mean strength or stiffness, but increasing the fiber loading further was associated with greater water absorption without additional improvement in these mechanical properties. The SEM and FTIR findings help explain some of these trends, particularly the changes around the fiber–matrix interface and the hydrophilic nature of OPMF. Even so, the contribution of each factor is not yet clear from the present results and would need further investigation.

4. Conclusions

The incorporation of waste-derived oil palm mesocarp fiber (OPMF) produced different responses in the strength, stiffness, and moisture-related behavior of LLDPE biocomposites. The 5 wt% OPMF composite showed the highest mean tensile and flexural strengths, reaching 16.16 ± 1.14 MPa and 29.33 ± 3.57 MPa, respectively, while the highest apparent tensile modulus and flexural modulus were obtained at 10 wt% OPMF. Increasing the fiber content also increased 24 h water absorption from 0.06 ± 0.01% for neat LLDPE to 1.19 ± 0.12% at 15 wt% OPMF, accompanied by a decrease in apparent water contact angle from 97.78 ± 2.04° to 65.18 ± 5.21°. The FTIR spectra showed the expected lignocellulosic-related features after OPMF was added, but no clear new bands were observed that would indicate new covalent bonding. The DSC results showed only minor changes in the melting and crystallization temperatures. The SEM images also showed several local fracture features, including fiber pull-out, separation at the fiber–matrix interface, and matrix tearing. Overall, the results show that the loading associated with higher strength was not the same as that giving the highest stiffness, while moisture sensitivity increased with OPMF content. These results suggest a low-loading performance window for waste-derived OPMF/LLDPE biocomposites.

Author Contributions: Conceptualization, M.I.N. and R.D.W.; methodology, M.I.N., R.D.W. and M.A.M.; validation, R.D.W., M.A.M., G.N. and B.S.E.P.; formal analysis, M.I.N., H.N.F., R.A.A. and U.A.S.; investigation, M.I.N., A.M., H.N.F. and R.A.A.; resources, R.D.W., G.N. and M.A.M.; data curation, M.I.N., H.N.F. and R.A.A.; writing—original draft preparation, M.I.N., A.M. and B.S.E.P.; writing—review and editing, R.D.W., A.M., B.S.E.P., E.P., U.A.S., G.N. and M.A.M.; visualization, M.I.N., H.N.F. and R.A.A.; supervision, R.D.W., M.A.M. and G.N.; project administration, M.I.N.,

H.N.F. and R.D.W.; funding acquisition, M.I.N. and R.D.W. All authors have read and agreed to the published version of the manuscript.

Funding: This research was funded by Universitas Negeri Semarang (UNNES), Indonesia.

Data Availability Statement: The original contributions presented in this study are included in the article. Further inquiries can be directed to the corresponding author.

Acknowledgments: The authors would like to express their sincere gratitude to Universitas Negeri Semarang (UNNES) and the Institute for Research and Community Service (LPPM), Universitas Negeri Semarang, for their support in providing Article Processing Charge (APC) assistance for the publication of this article. During the preparation of this manuscript, the authors used ChatGPT (GPT-6; OpenAI) and Grammarly (web version; Grammarly, Inc.) to refine language, improve grammatical accuracy, enhance clarity, and assist in organizing selected sections of the manuscript. The authors have reviewed and edited the output and take full responsibility for the content of this publication.

Conflicts of Interest: The authors declare no conflicts of interest.

References

1. Sayam, S. Natural fibers in sustainable materials: Extraction technologies, fiber modification, and performance–sustainability relationships. *RSC Adv.* **2026**, *16*, 10495–10537. [CrossRef]
2. Roy, I.; Andrew, J.J.; Misra, M.; Mohanty, A.K.; Sharma, A.K.; Dhakal, H.N. A review on sustainable bamboo fibre composites in construction: Recent advancements, properties and future perspectives. *Compos. Part C Open Access* **2026**, *20*, 100716. [CrossRef]
3. Bonyani, M.; Marincic, I.C.; Krishnan, S. Advancing Sustainable Materials Engineering with Natural-Fiber Biocomposites. *J. Compos. Sci.* **2026**, *10*, 86. [CrossRef]
4. Widodo, R.D.; Nuryanta, M.I.; Handayani, P.A.; Ichwan, R.; Zainudin, E.S.; Muflikhun, M.A. Sustainable Hybrid Laminated Composites Reinforced with Bamboo, Flex Banner, and Glass Fibers: Impact of $CaCO_3$ Filler on Mechanical Properties. *Polymers* **2026**, *18*, 275. [CrossRef]
5. Nadeem, M.M.; Mozumder, M.S.; Saba, N.; Ismail, A.S.; Jawaid, M. Effect of kenaf and oil palm fibers on the mechanical, physical and morphological properties of the bio-epoxy hybrid composites. *J. Mater. Res. Technol.* **2025**, *38*, 3472–3481. [CrossRef]
6. Saepoo, T.; Mayakun, S.; Eksomtramage, J.; Kaewtatip, T. Thermoplastic starch composite with oil palm mesocarp fiber waste and its application as biodegradable seeding pot. *Carbohydr. Polym.* **2023**, *299*, 120221. [CrossRef]
7. Widodo, R.D.; Nuryanta, M.I.; Fitriyana, D.F.; Rusiyanto; Firmansyah, H.N.; Widayat, W.; Kriswanto; Darsono, F.B.; Mujaki, A.; Muflikhun, M.A. The influence of flex banner types on the impact and flexural strength of hybrid composite materials. *J. Phys. Conf. Ser.* **2025**, *3103*, 012035. [CrossRef]
8. Huisken, P.W.; Tchemou, G.; Tagne, N.R.S.; Ndapeu, D.; Njeugna, E. Effect of the Addition of Oil Palm Mesocarp Fibers on the Physical and Mechanical Properties of a Polyester Matrix Composite. *Int. J. Polym. Sci.* **2022**, *2022*, 3399986. [CrossRef]
9. Mahardika, M.; Zakiyah, A.; Ulfa, S.M.; Ilyas, R.A.; Hassan, M.Z.; Amelia, D.; Knight, V.F.; Norrrahim, M.N.F. Recent Developments in Oil Palm Empty Fruit Bunch (OPEFB) Fiber Composite. *J. Nat. Fibers* **2024**, *21*, 2309915. [CrossRef]
10. Rotkovich, A.A.; Tishkevich, D.I.; Razanau, I.U.; Vershinina, T.N.; Bondaruk, A.A.; German, S.A.; Zubar, T.I.; Sayyed, M.I.; Dong, M.; Yao, Y.; et al. Development and study of lightweight recycled composite materials based on linear low-density polyethylene and W for radiation application. *J. Mater. Res. Technol.* **2024**, *30*, 1310–1318. [CrossRef]
11. Yadav, J.; Ramkumar, P.; Parwani, A.K. Transforming fly ash into value: Sustainable LLDPE-fly ash composites via rotational molding. *J. Thermoplast. Compos. Mater.* **2025**, *38*, 3219–3241. [CrossRef]
12. Wasti, S.; Clarkson, C.; Johnston, E.; Pu, Y.; Bhagia, S.; Tekinalp, H.; Ozcan, S.; Vaidya, U. Sizing of discontinuous natural fibers: Effect of sizing approach and sizing concentration on composite properties. *Compos. Part A Appl. Sci. Manuf.* **2025**, *197*, 109029. [CrossRef]
13. Nuryanta, M.I.; Widodo, R.D.; Samsudi, S.; Ramadiani, F.R.; Mujaki, A.; Zainudin, E.S.; Muflikhun, M.A. Loading-mode-dependent mechanical response and moisture behavior of liquid-asphalt-modified cotton/bamboo hybrid epoxy composites fabricated by vacuum infusion. *Mater. Today Commun.* **2026**, *57*, 116287. [CrossRef]
14. Mohammed, M.; Rahman, R.; Mohammed, A.M.; Adam, T.; Betar, B.O.; Osman, A.F.; Dahham, O.S. Surface treatment to improve water repellence and compatibility of natural fiber with polymer matrix: Recent advancement. *Polym. Test.* **2022**, *115*, 107707. [CrossRef]
15. Adam, H.M.; Bekele, A.A. Synergistic effects of nanofillers on treated natural fiber composites: A comprehensive review of mechanical and moisture resistance enhancement. *Next Mater.* **2026**, *12*, 102080. [CrossRef]

16. Elfaleh, I.; Abbassi, F.; Habibi, M.; Ahmad, F.; Guedri, M.; Nasri, M.; Garnier, C. A comprehensive review of natural fibers and their composites: An eco-friendly alternative to conventional materials. *Results Eng.* **2023**, *19*, 101271. [CrossRef]
17. Chen, X.; Wang, X.; Luo, X.; Chen, L.; Li, Y.; Xu, J.; Liu, Z.; Dai, C.; Miao, H.; Liu, H. Bamboo as a naturally-optimized fiber-reinforced composite: Interfacial mechanical properties and failure mechanisms. *Compos. Part B Eng.* **2024**, *279*, 111458. [CrossRef]
18. Nuryanta, M.I.; Sentanuhady, J.; Muflikhun, M.A. Moisture absorption behavior of hybrid composite laminates consist of natural and glass fiber. *Mater. Today Proc.* **2022**, *66*, 2924–2928. [CrossRef]
19. Olusunmade, O.F.; Adetan, D.A.; Ogunnigbo, C.O. A Study on the Mechanical Properties of Oil Palm Mesocarp Fibre-Reinforced Thermoplastic. *J. Compos.* **2016**, *2016*, 3137243. [CrossRef]
20. Hanipah, S.H.; Omar, F.N.; Talib, A.T.; Mohammed, M.A.P.; Baharuddin, A.S.; Wakisaka, M. Effect of Silica Bodies on Oil Palm Fibre-Polyethylene Composites. *BioResources* **2020**, *15*, 360–367. [CrossRef]
21. Ritonga, A.H.; Sisca, V.; Aritonang, B.; Meilani, D.; Putri, G.E.; Siahaan, E.W.B. Integrated PLA/LLDPE nanocomposites with compatibilizer and hydroxyapatite-zinc oxide: Mechanical, physical, thermal, and morphological properties, South African. *J. Chem. Eng.* **2025**, *52*, 1–7. [CrossRef]
22. Chaves, Y.S.; da Silveira, P.H.P.M.; Neuba, L.d.M.; Junio, R.F.P.; Ribeiro, M.P.; Monteiro, S.N.; Nascimento, L.F.C. Evaluation of the density, mechanical, thermal, and chemical properties of babassu fibers (*Attalea speciosa*) for potential composite reinforcement. *J. Mater. Res. Technol.* **2023**, *23*, 2089–2100. [CrossRef]
23. Rajendran, S.; Veerasimman, A.; Shanmugam, V.; Yang, Y.-L.; Marimuthu, U.; Sundaresan, T.K.; Karuppiah, K. Water Absorption and Mechanical Durability of Ramie–Flax Fibre-Reinforced Epoxy Hybrid Composites. *J. Compos. Sci.* **2026**, *10*, 175. [CrossRef]
24. Ses, B.; Polonia, E.; Waluyo, J.; Fikry, M.J.M.; Yuswanda, I.; Akhsin, M. Journal of Water Process Engineering Abiomimetic leaf epidermis: Moldable knitted fabric based carbon fiber evaporator using weaving process for stable solar water desalination. *J. Water Process Eng.* **2026**, *93*, 110910. [CrossRef]
25. *ASTM D638-22*; Standard Test Method for Tensile Properties of Plastics. ASTM International: West Conshohocken, PA, USA, 2022.
26. Widodo, R.D.; Nuryanta, M.I.; Handayani, P.A.; Ichwan, R.; Zainudin, E.S.; Muflikhun, M.A. Property relationships study of sugar palm fiber-reinforced recycled HDPEbottle-cap composites. *J. Mater. Res. Technol.* **2026**, *42*, 4311–4323. [CrossRef]
27. *ASTM D790-25*; Standard Test Methods for Flexural Properties of Unreinforced and Reinforced Plastics and Electrical Insulating Materials. ASTM International: West Conshohocken, PA, USA, 2025.
28. Nuryanta, M.I.; Aryaswara, L.G.; Korsmik, R.; Klimova-Korsmik, O.; Nugraha, A.D.; Darmanto, S.; Kusni, M.; Muflikhun, M.A. The Interconnection of Carbon Active Addition on Mechanical Properties of Hybrid Agel/Glass Fiber-Reinforced Green Composite. *Polymers* **2023**, *15*, 2411. [CrossRef]
29. Endesha, A.; Tefera, G.; Adali, S.; Bright, G. The Effects of Extraction on Mechanical Morphological Properties of Sisal Polyester Composite. *J. Compos. Sci.* **2025**, *9*, 613. [CrossRef]
30. Grine, M.; Slamani, M.; Amroune, S.; Nyiranzeyimana, G.; Seki, Y.; Louhichi, B.; Elfar, A.A. FTIR Spectra and Tensile Strength Analysis of Alkali-Treated Alfa Fiber (*Stipa tenacissima* L.) Reinforced Polyester Composites with Uncertainty Quantification Due to Natural Fiber Variability. *J. Nat. Fibers* **2026**, *23*, 2691824. [CrossRef]
31. K, S.; Brn, M.; Hiremath, A.; Singh, M.K.; Palaniappan, S.K.; Rangappa, S.M.; Siengchin, S. Investigation of thermo-mechanical and tribological performance of zirconia-coated MWCNTs reinforced HDPE composites. *Constr. Build. Mater.* **2025**, *496*, 143830. [CrossRef]
32. Huisken Mejouyo, P.W.; Harzallah, O.; Sikame Tagne, N.R.; Ndapeu, D.; Tchemou, G.; Drean, J.Y.; Njeugna, E. Physical and Mechanical Characterization of Several Varieties of Oil Palm Mesocarp Fibers Using Different Cross-Sectional Assumptions. *J. Nat. Fibers* **2021**, *18*, 175–191. [CrossRef]
33. Klippathum, C.; Kunawisarut, A.; Chuaicham, C.; Jirawattanasomkul, T.; Likitlersuang, S.; Dai, J.-G.; Jongvivatsakul, P. Tensile performance and carbon intensity of natural fiber–reinforced polymer composites using bio-based epoxy resins. *J. Mater. Res. Technol.* **2026**, *42*, 6722–6741. [CrossRef]
34. Ajayi, N.E.; Rusnakova, S.; Ajayi, A.E.; Ogunleye, R.O.; Agu, S.O.; Amenaghawon, A.N. A comprehensive review of natural fiber reinforced Polymer composites as emerging materials for sustainable applications. *Appl. Mater. Today* **2025**, *43*, 102666. [CrossRef]
35. Kargar, E.; Hosseini-Taklimi, S.-A.; Ghasemi-Ghalebahman, A. Fracture behavior of sustainable wood and PLA composites fabricated by fused deposition modeling using essential work of fracture. *Sci. Rep.* **2025**, *15*, 34929. [CrossRef]
36. Tazwar, H.T.; Antora, M.F.; Rahman, M.Z. Functionalization strategies for sustainable plant fiber composites: Acomprehensive review of techniques performance and future directions. *J. Mater. Res. Technol.* **2025**, *38*, 1083–1102. [CrossRef]
37. Chen, J.; Pan, Z.; Yang, S.; Cao, C.; Zhou, W.; Xie, Y.; Yang, Y.; Qian, Q.; Chen, Q. Highly Filled Waste Polyester Fiber/Low-Density Polyethylene Composites with a Better Fiber Length Retention Fabricated by a Two-Rotor Continuous Mixer. *Polymers* **2024**, *16*, 2929. [CrossRef]
38. Özyer, T.; Demirci, E. Evaluation of Jute–Glass Ratio Effects on the Mechanical, Thermal, and Morphological Properties of PP Hybrid Composites for Sustainable Automotive Applications. *Polymers* **2025**, *17*, 3335. [CrossRef]

39. Asthana, A.; Srinivas, R.; Chauhan, S.S.; Bandhu, D.; Dwivedi, S.P.; Saxena, K.K.; Kaur, K.; Alnaser, I. Development and mechanical properties evaluation of environmentally sustainable composite material using various reinforcements with epoxy. *Case Stud. Constr. Mater.* **2024**, *21*, e03624. [CrossRef]
40. Rangappa, S.M.; Siengchin, S.; Parameswaranpillai, J.; Jawaid, M.; Ozbakkaloglu, T. Lignocellulosic fiber reinforced composites: Progress, performance, properties, applications, and future perspectives. *Polym. Compos.* **2022**, *43*, 645–691. [CrossRef]
41. Adam, H.M.; Bogale, T.M.; Paramasivam, V. Natural Fiber Composites Under Dynamic Loading: A Comprehensive Review of Mechanical Performance and Structural Integrity. *Eng. Rep.* **2026**, *8*, e70722. [CrossRef]
42. Muñoz-Acosta, F.; Gaitán-Álvarez, J.; Arias-Aguilar, D.; Valverde, J.C.; Garro-Monge, G.; Mora-Molina, J. Improvement in the physical and mechanical properties of polyethylene and recycled polypropylene composites reinforced with Musa textilis fiber. *Discov. Mater.* **2026**, *6*, 48. [CrossRef]
43. Widodo, R.D.; Nuryanta, M.I.; Syafei, M.H.G.; Rohman, S.; Mujaki, A.; Darsono, F.B.; Muflikhun, M.A. Impact and Flexural Response of Hybrid Composite Consisting of Waste Flex Banner and Glass Fiber Jordan. *J. Mech. Ind. Eng.* **2025**, *19*, 749–761. [CrossRef]
44. Nuilek, K.; Somdee, P.; Homjabok, W.; Bunon, C.; Shettar, M. Influence of Alkali-Treated Hemp Stem Fiber on the Structure, Properties, and Soil Biodegradation of Poly(butylene succinate)/Poly(lactic acid) Biocomposites. *J. Compos. Sci.* **2026**, *10*, 389. [CrossRef]
45. Silva, D.S.; Aguilera, L.D.S.; Junio, R.F.P.; Monteiro, S.N.; da Silva, M.H.P. Mechanical Properties of Raffia Fiber Fabric (Raphia vinifera)-Reinforced Epoxy Matrix Composites. *J. Compos. Sci.* **2025**, *9*, 504. [CrossRef]
46. Soesanti, A.; Batan, I.M.L.; Wahjudi, A.; Effendi, M.K.; Izzuddin, M.Y.; Suwarta, P. Effect of fiber type and fiber loading on the mechanical behavior and microstructure of natural fiber reinforced polymer composites. *Results Mater.* **2026**, *31*, 101023. [CrossRef]
47. Maziarz, W.; Chulist, R.; Chyzhyk, G.; Wojcik, A.; Kurtyka, P.; Sobula, S.; Schell, N.; Olejnik, E. Effect of microstructural heterogeneity on the strengthening and fracture mechanism in in-situ cast TiC/Al composites. *Mater. Des.* **2026**, *264*, 115756. [CrossRef]
48. Dascanio, R.; Kury, M.; Fronza, B.M.; Cavalli, V.; Özcan, M. Filler-Matrix Interface Engineering in Resin Composites: Fundamentals, Strategies, and Critical Gaps. *Curr. Oral Health Rep.* **2026**, *13*, 6. [CrossRef]
49. Fang, H.; Xi, L.; Huang, Y.; Zhao, T.; He, R.; Kang, X.; Li, Y.; Fang, D. Fiber-reinforced composites: A comprehensive review of traditional and additive manufacturing processes and material architectures. *Compos. Part A Appl. Sci. Manuf.* **2026**, *205*, 109684. [CrossRef]
50. Prasetya, R.; Gapsari, F.; Andoko, A.; Anam, K.; Raharjo, R.; Rangappa, S.M.; Siengchin, S. Moisture-induced swelling in natural fiber-reinforced composites: A critical review of chemical treatments, hybrid strategies, and environmental durability. *Green Technol. Sustain.* **2026**, *4*, 100336. [CrossRef]
51. Mohammadi, M.; Ishak, M.R.; Sultan, M.T.H. Exploring Chemical and Physical Advancements in Surface Modification Techniques of Natural Fiber Reinforced Composite: A Comprehensive Review. *J. Nat. Fibers* **2024**, *21*, 2408633. [CrossRef]
52. Aris, N.F.; Ghazali, S.K.; Mohamad, Z.; Jamaluddin, J.; Adrus, N.; Abdul Aziz, A.; Low, J.H.; Majid, R.A. The effects of alkaline treatment on the oil residue, thermal properties and surface morphology of oil palm mesocarp fiber. *Environ. Qual. Manag.* **2022**, *32*, 405–411. [CrossRef]
53. Saifullah, A.; Rahman, A.; Reza, S.; Joseph, J.; Wang, L.; Pickford, A.R.; Dhakal, H.N. Date Palm Fiber Agricultural Residue Valorization in Rotationally Molded LLDPE Single- and Multilayered Composites for Engineering Applications. *ACS Omega* **2026**, *11*, 50853–50870. [CrossRef]
54. Zakaria, M.K.; Muhamad, M.; Yew, B.S.; Mohamed, S.B.; Millar, B.; Douglas, P. Impact of banana fibers and compatibilizer loadings on the tensile, microstructural and morphological characteristics of high-density polyethylene (HDPE) composites. *Iran. Polym. J.* **2026**, *advance online publication*. [CrossRef]
55. Bosenbecker, M.W.; Silva, E.V.; Paganotto, G.F.d.R.; Zanon, T.T.M.; Langone, F.; Rodrigues, M.B.B.; Marini, J.; Labidi, J.; Missio, A.L.; de Oliveira, A.D. Effect of different compatibilizers on the properties of green low-density polyethylene composites reinforced with Bambusa vulgaris bamboo fibers. *Polymers* **2024**, *16*, 1760. [CrossRef]
56. Siddiqui, V.U.; Sapuan, S.M.; Isah, A.; Yusuf, J.; Khan, A. Advancements in multiscale oil palm fiber composites: Manufacturing techniques, performance evaluation, and industrial applications. *Ind. Crops Prod.* **2024**, *213*, 118399. [CrossRef]

Disclaimer/Publisher's Note: The statements, opinions and data contained in all publications are solely those of the individual author(s) and contributor(s) and not of MDPI and/or the editor(s). MDPI and/or the editor(s) disclaim responsibility for any injury to people or property resulting from any ideas, methods, instructions or products referred to in the content.